CHAPTER V

RESULTS AND DISCUSSION OF GaAsN/GaAs MULTIQUANTUM WELLS

In this chapter, we describe optical and structural properties of GaAsN/GaAs multiple quantum wells (MQWs), which were investigated by photoluminescence (PL), high-resolution X-ray diffraction (HRXRD) and transmission electron microscopy (TEM). In order to improve structural and optical properties of the GaAsN alloy with higher N concentrations, both the quantum well structure and post-growth thermal annealing were applied in the GaAsN alloy system. Both the QW structure and the annealing treatment demonstrate an improvement in both the structural quality and optical properties of the GaAsN/GaAs MQWs emitting at around 1.3 μm-wavelength. Moreover, the type of fundamental band alignment of the GaAsN/GaAs heterostructure system is also discussed.

5.1 Determination of Well Dimension and N Concentration

Firstly, in order to observe the interface and microstructure of GaAsN/GaAs MQWs, the TEM measurement was performed. Figure 5.1 presents a cross-sectional bright field TEM image of as-grown GaAsN/GaAs MQWs. The TEM image reveals the sharp and well-defined interfaces between the GaAsN wells and the GaAs barriers. No indication of misfit dislocations (MDs) and threading dislocations (TDs) at the interfaces between GaAsN well and GaAs barrier layers are observed. It reveals that the as-grown MQWs is coherently grown on the GaAs substrate. Thicknesses of the well and barrier layers obtained from the TEM image are estimated to be about 5.0 and 27.0 nm, respectively. To confirm the well dimension and the N concentration and get more detail of structural properties, the HRXRD measurements were carried out. Figure 5.2 (a) illustrates (004) HRXRD pattern obtained from the as-grown GaAsN/GaAs MQWs. It is clearly seen that the satellite peaks and Pendellösung fringes are clearly visible due to a finite thickness and high crystalline quality of the as-grown GaAsN/GaAs MQWs in spite of the high tensile strain in the QWs ($\Delta a/a$ = -

Figure 5.1: (a) Schematic diagram and (b) cross-sectional TEM image of as-grown GaAsN/GaAs 10-periods MQWs.

1.02%). The separation between the nearest neighbor's satellite peaks is quite constant, showing that flat hetero-interfaces and uniform well-thickness are achieved. Because the GaAsN (004) peak in diffraction pattern cannot be observed, so we are not able to directly calculate the N concentration. The technique which can be used to determine the N concentration in GaAsN well layer as well as the well and barrier thickness is a simulation method using dynamical-theory simulation software. The simulated conditions consist of (i) the strain in the well layer; in this case, the GaAsN layer is fully strained; (ii) the N concentration for adjusting satellite peak position; and (iii) the well and barrier thickness for changing the separation between the satellite peaks. In Fig. 5.2, curve b shows the dynamical-theory simulation result, in comparison to the experimental curve (a). From the simulation, the N concentration (x) is estimated to be $x = 0.050$. Thickness of the GaAsN well and GaAs barrier layers are also estimated to be 5.0 nm and 26.0 nm, respectively. The period of GaAsN/GaAs stack becomes 31.0 nm, which is well comparable to the values determined from the cross-sectional TEM image. Based on TEM and HRXRD results, it is evident that a high epitaxial quality and coherently strained $GaAs_{1-x}N_x$/GaAs MQWs with N concentration as high as $x = 0.050$ was successfully grown by MOVPE.

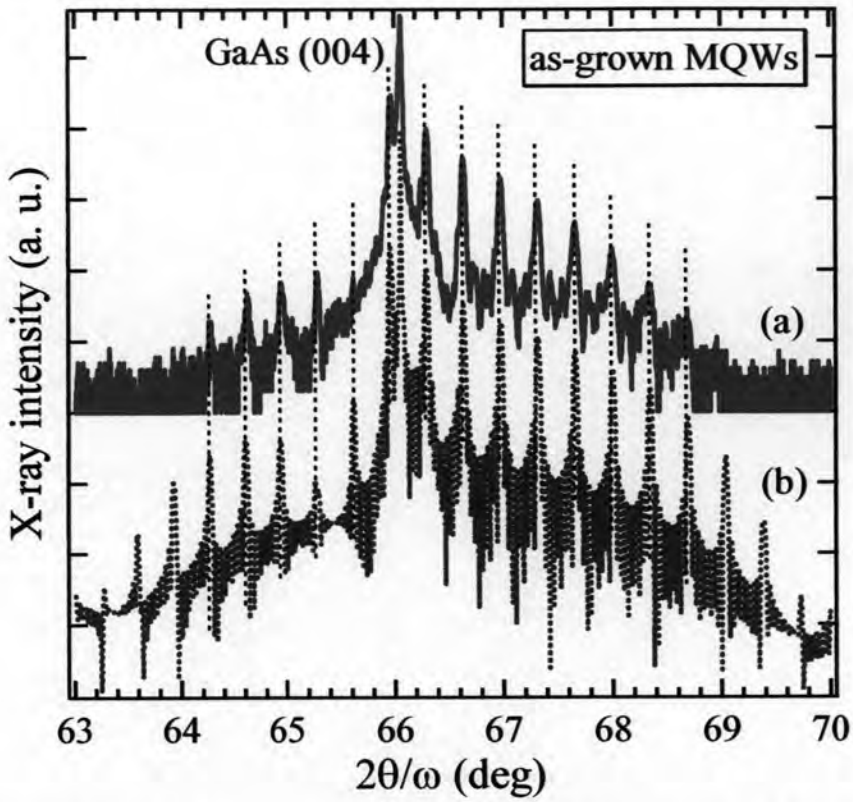

Figure 5.2: (004) XRD patterns of as-grown $GaAs_{0.950}N_{0.050}$/GaAs 10-periods MQWs. The (a) solid curve is the experimental data and (b) the dashed curve is a simulation result using the dynamical-theory software.

5.2 Optical Investigation

Figure 5.3 shows low-temperature (10 K) PL results of the as-grown $GaAs_{0.950}N_{0.050}$/GaAs MQWs and a reference $GaAs_{0.949}N_{0.051}$ bulk layer, which was annealed at 650°C for 2 min. Note that the PL emission from the as-grown bulk layer cannot be detected because of the highly non-radiative recombination centers in such high N-containing layer. After post-growth thermal annealing, a single PL peak emission is clearly observed at about 0.96 eV, which corresponds to the long wavelength emission at about 1.3 μm. This indicates that the annealing process can improve optical quality of such high N-containing GaAsN bulk layer. On the other hand, strong PL emission obtained from as-grown MQWs is observed. This reveals that the optical quality can also be improved by QW structures. In comparison with the annealed bulk layer, the PL peak energy of the as-grown MQWs blue shifts amounts to 80 meV. This large PL blue-shift is believed to be predominantly

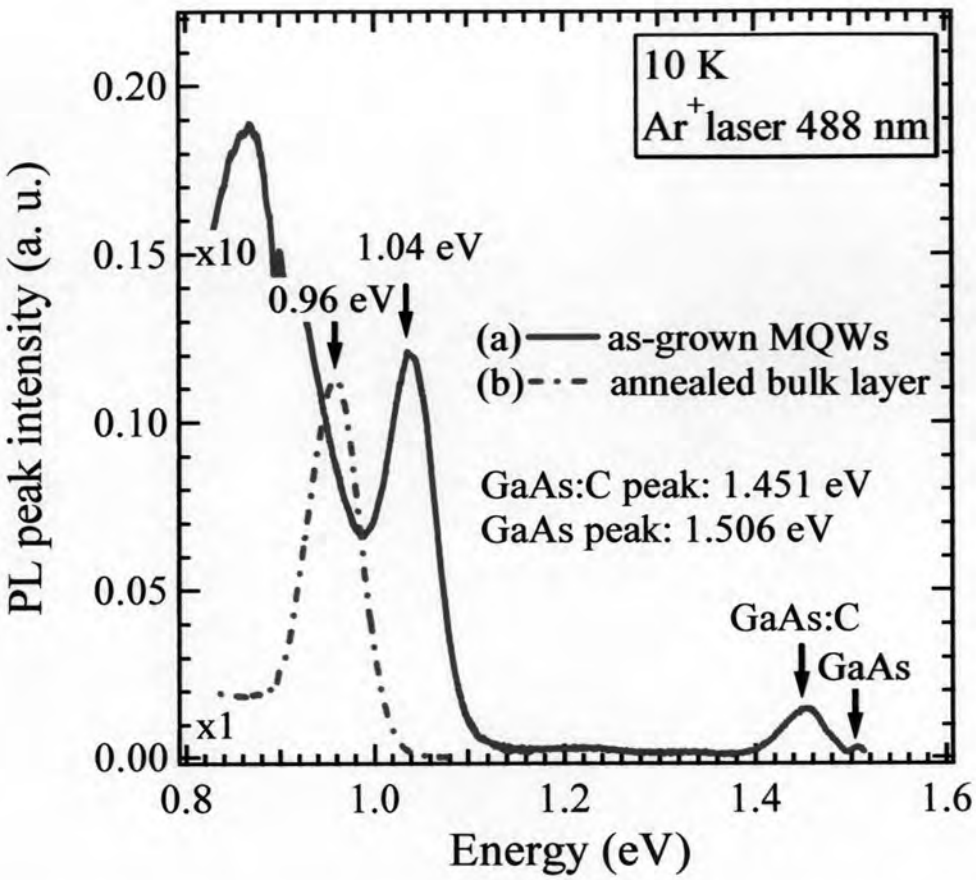

Figure 5.3: Low-temperature (10K) PL spectra of (a) as-grown $GaAs_{0.950}N_{0.050}$/GaAs MQWs and (b) reference $GaAs_{0.949}N_{0.051}$ bulk layer, which was annealed at 650°C for 2 min.

determined by the strong quantum confinement effect to the well. The PL emission from the as-grown MQWs is observed at about 1.04 eV. The PL emission from the as-grown MQWs has a broad spectrum in the low energy region centered at 0.85 eV. In addition, PL peaks at 1.451 and 1.506 eV are related to carbon-accepter [10] and free exciton states of the GaAs [10], respectively. The incorporated carbon atoms in GaAs barriers are originated from methyl group of gas sources during growth process.

Additionally, the difference between the PL peak positions of the annealed bulk layer (0.96 eV) and the GaAs barrier (1.506 eV) is about 550 meV. It is known that additional of N atoms into GaAs decreases the bandgap energy, which mainly affects the conduction band (CB) and only a small valence band discontinuity ($\Delta E_V \sim 0$) [44]. Thus, the difference result is approximated to be a large conduction band

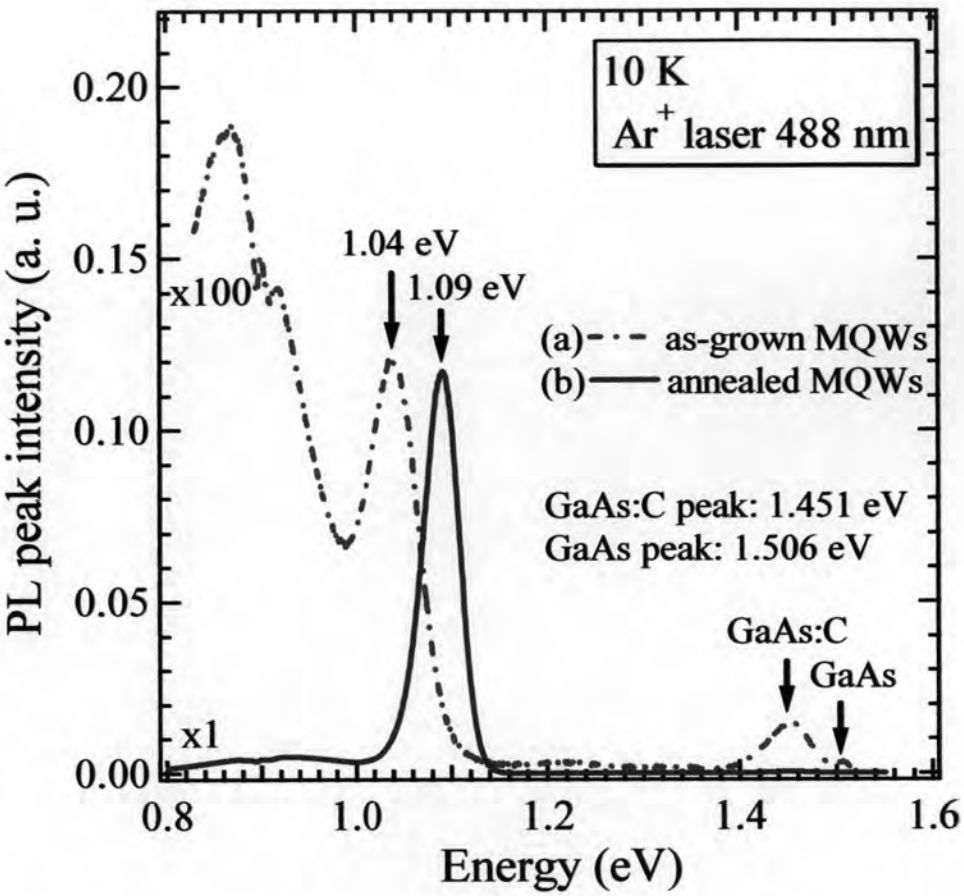

Figure 5.4: Low-temperature (10K) PL spectra of (a) the as-grown and (b) the annealed MQWs.

offset (ΔE_C ~ 550 meV), which is realized in $GaAs_{1-x}N_x$/GaAs heterostructure. This result demonstrates an efficient carrier confinement, which is realized in the high N-containing $GaAs_{1-x}N_x$/GaAs MQWs, giving higher efficient PL emission at higher temperatures. Comparing with the annealed bulk layer, the PL peak intensity of as-grown MQWs is lower than that of the annealed bulk layer about 10 times. This result shows low efficiency of PL intensity due to the highly non-radiative recombination centers. Based on our early band alignment type calculation (see detail in section 2.2.4), it is indicated that the band alignment of GaAsN/GaAs heterostructure is a type-II band lineup (indirect recombination). This can suggest that the low efficiency of PL peak may be originated from the indirect recombination for GaAsN/GaAs type-II band lineup. In order to improve the PL efficiency by the removal of the non-radiative recombination centers, the post-growth thermal annealing was carried out.

5.3 Post-Growth Thermal Annealing Effects on Optical Property

Low-temperature (10 K) PL spectra of the (a) as-grown and (b) annealed $GaAs_{0.950}N_{0.050}$/GaAs MQWs are shown in Fig. 5.4. After annealing, the peak intensity of the quantum well emission is increased by a factor of 100, indicating the improvement of optical quality induced by the reduction of non-radiative recombination centers. It is known that the increase in PL peak intensity by annealing process can improve optical property of GaAsN alloy by a factor of 30 [40]. Thus, another reason for supporting the increase in PL peak intensity after post-growth thermal annealing may be originated from the transformation of recombination process from indirect to direct recombination (transformation from type-II to type-I band lineup). In addition, the PL peak position shows a blue-shift of approximately 50 meV from 1.04 to 1.09 eV. In general for GaAsN bulk layer, this blue-shift of PL peak position suggests that the annealing process induces (i) diffusion of N atoms out of the well layers, (ii) strain relaxation in the GaAsN well layer, and (iii) homogeneity of the localization potential due to the N distribution fluctuations. In case of the GaAsN/GaAs type-II QWs, one way that can encourage blue-shift of PL peak is the transformation from indirect to direct recombination.

To make clear this point, the (115) reciprocal mapping measurement was also performed to determine the N concentration, strain state and the well dimension in annealed layer, the (004) HRXRD measurement and simulation method were also done. Figure 5.5 shows the (004) HRXRD patterns, which obtained from (a) as-grown, (b) annealed (650°C, 2 min) $GaAs_{0.950}N_{0.050}$/GaAs MQWs, and (c) simulation result using the dynamical-theory software for annealed MQWs. The satellite peaks and Pendellösung fringes are still clearly visible for the annealed MQWs, as shown in Fig. 5.5 (b). These results indicate that both the high N-containing as-grown and annealed MQWs are coherently strained without any indication of strain relaxation. In Fig. 5.5 (b), the post-growth thermal annealing results in a shift of the satellite peaks to a lower diffraction angle, indicating a reduction of the N concentration in the well, which is verified by the dynamical-theory simulation results. The fitted N concentration (x) inside the annealed GaAsN well layer is reduced to $x = 0.048$. The reduction of N concentration is also clearly observed, indicating the diffusion of N

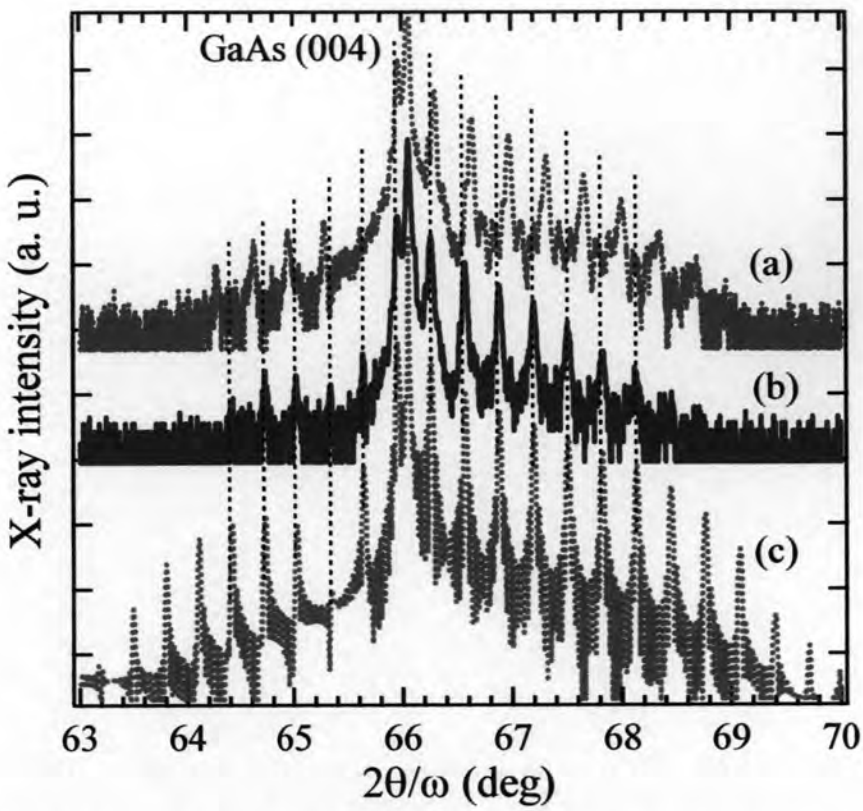

Figure 5.5: (004) HRXRD patterns of (a) as-grown, (b) annealed 10-periods $GaAs_{0.950}N_{0.050}$/GaAs MQWs. (c) showing a simulation result using the dynamical-theory software for the annealed MQWs.

atoms out of the well layers during thermal post annealing. Furthermore, it is also found that the separation between the nearest neighbor's interference fringes is quite the same as the as-grown sample. This suggests that there is no change in the thicknesses of the well layer. According to fitting results, the thickness of the well and barrier layers are determined to be 5.0 and 27.0 nm, respectively.

Based on the HRXRD results as shown in Fig. 5.5, in the present case, the blue-shift of PL peak position indicates that the annealing process induces diffusion of N atoms out of the well layers and homogeneity of the localization potential due to the N distribution fluctuations. No strain relaxation in the GaAsN well layers is clearly observed. Moreover, this blue-shift may be originated by the transformation of indirect to direct recombination. This reason quite corresponds to the increase in PL intensity after annealing. It is also evident that after annealing the full width at half

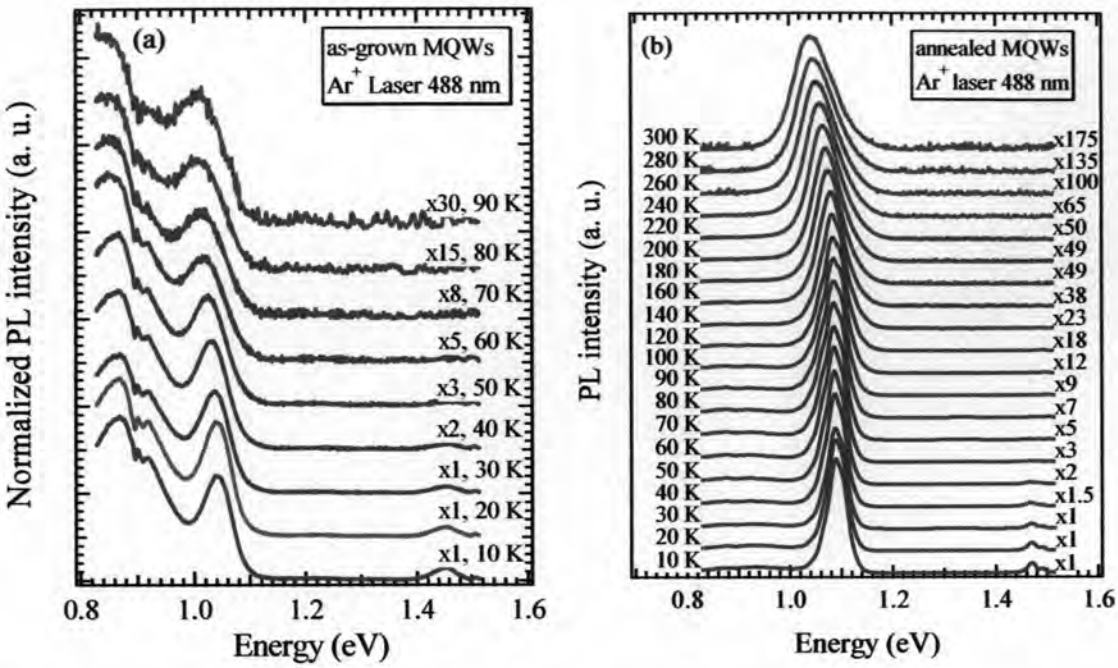

Figure 5.6: Temperature dependence of PL spectra for (a) as-grown and (b) annealed $GaAs_{0.950}N_{0.050}$/GaAs MQWs.

maximum (FWHM) of PL peak is decreased from 72 to 43 meV, confirming the improvement of composition uniformity.

To understand the origin of PL transition obtained from the $GaAs_{1-x}N_x$/GaAs MQWs, the temperature dependence of PL spectra and calculated transition energy in the well are compared.

5.4 Temperature-dependent PL

Figure 5.6 shows temperature dependence of PL spectra for (a) as-grown and (b) annealed MQWs. In case of as-grown MQWs, as shown in Fig. 5.6(a), the PL spectra can be only detected ranging from 10 K to 90 K due to high non-radiative defects, indicating the low optical efficiency with increasing temperature. However, for annealed MQWs (Fig. 5.6(b)), the PL spectra can be detected ranging from 10 K to 300 K, indicating the higher optical efficiency than the as-grown MQWs, and indicating that annealing process can remove the non-radiative defects. First, to know the optical transition in GaAsN/GaAs QWs, we will compare the temperature

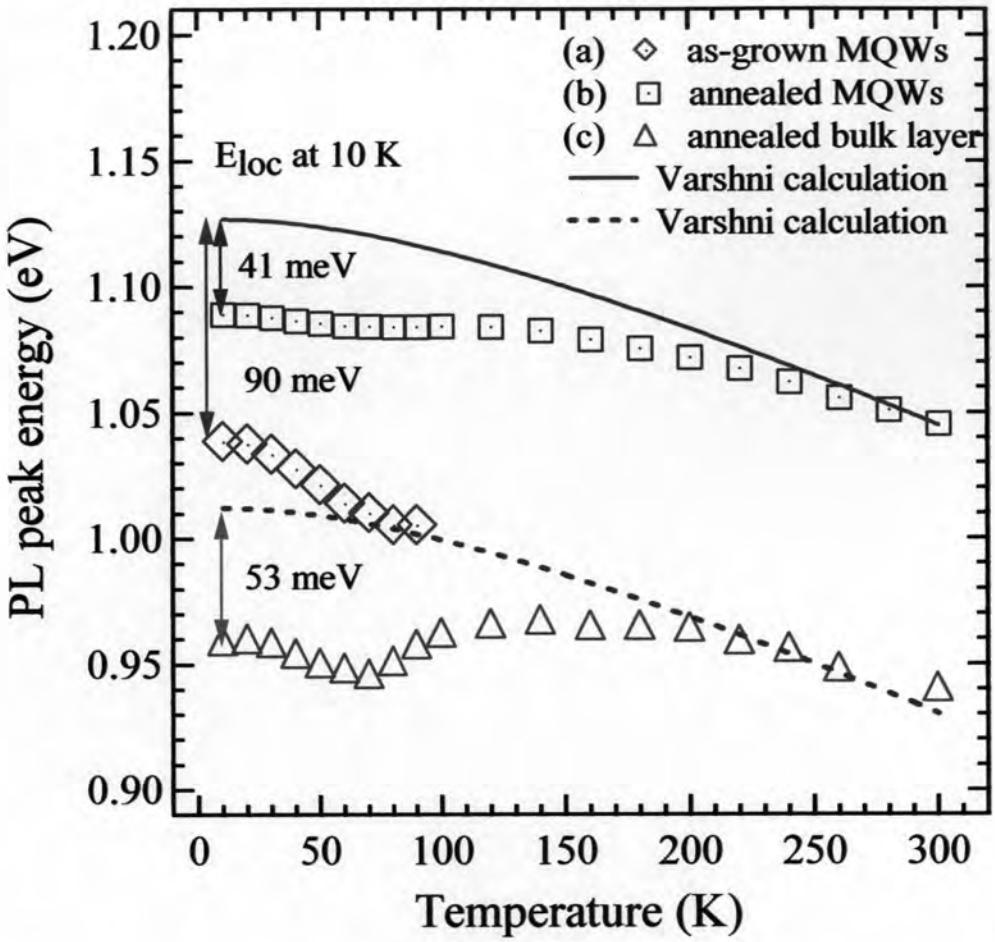

Figure 5.7: Temperature variation of PL peak energies for (a) as-grown, (b) annealed $GaAs_{0.950}N_{0.050}$/GaAs MQWs and (c) annealed $GaAs_{0.949}N_{0.051}$ bulk layer. The solid and dashed curves denote the temperature dependence of bandgap energy of $GaAs_{0.952}N_{0.048}$ and $GaAs_{0.949}N_{0.051}$ alloys using empirical Varshni model calculation, respectively.

dependence of PL peak position of annealed $GaAs_{0.952}N_{0.048}$/GaAs MQWs and those of $GaAs_{0.952}N_{0.048}$ alloy calculated by Varshni model.

Figure 5.7 reveals the temperature dependence of PL peak position of as-grown and annealed MQWs. The solid line denotes the calculated bandgap energy of $GaAs_{0.952}N_{0.048}$ layer. Based on GaAsN bulk layer, it is known that at high temperature, the PL peak position is originated from the bandgap energy of GaAsN alloy. In Fig. 5.7, at 300K the solid line or bandgap energy of $GaAs_{0.952}N_{0.048}$ layer is shifted to be coincident with the PL peak position of annealed MQWs. In comparison

between the temperature dependence of PL peak position and calculated bandgap energy of annealed MQWs, demonstrates that the PL peak position is not originated from the bandgap energy at low temperature. This indicates that the transition process is attributed to the localized energy states. The localization energy in GaAsN/GaAs MQW is caused by the conduction band edge fluctuation and well width fluctuation due to local alloy uniformity. Although the PL signal of as-grown MQWs cannot be detected over the entire temperature range, the temperature dependence of PL peak position is expected to change in a similar way with the annealed MQWs. If the difference between the PL peak position and bandgap energy at 10 K is estimated to be the localization energy, the localization energy is approximated to be 90 and 41 meV for as-grown and annealed MQWs, respectively, as shown in Fig. 5.7. This suggests that the annealing process homogenizes the N distribution in the well layers, resulting in the reduction of localization energy. This also confirms that the composition uniformity can be improved by the annealing process. Moreover, the tendency of changing in PL peak position of annealed MQWs with temperature is comparable with the temperature dependence of PL peak position of annealed bulk layer. The localization energy at 10 K of annealed MQWs (41 meV) is the same order of magnitude to that of the annealed bulk layer (53 meV), indicating that the same annealing conditions (650°C, 2 min) can improve the optical quality in the same order scale for both annealed bulk layer and annealed MQWs. In the case of annealed MQWs, the temperature dependence of PL peak position is S-shaped. Then, the mechanism of transference of carriers between localization potential in the annealed MQWs can be described in the same way as that in the GaAsN bulk layer.

Based on the calculation in section 2.2.4, the band alignment of GaAsN/GaAs QWs system is a type-II band lineup. As a result, we calculate the transition energy from GaAsN/GaAs type-II band lineup to compare with the PL peak position.

5.5 Examination of Band Alignment

In order to calculate the transition energy in the well, the conduction band offset (ΔE_C) is a required parameter to know the barrier height for confining carrier. We assume that the ΔE_C is constant at every temperature. Thus, the ΔE_C is calculated at 10 K. For GaAsN/GaAs type-II QWs, the $\Delta E_C = E_{g,GaAs} + \Delta E_V - E_{g,GaAsN}$. The

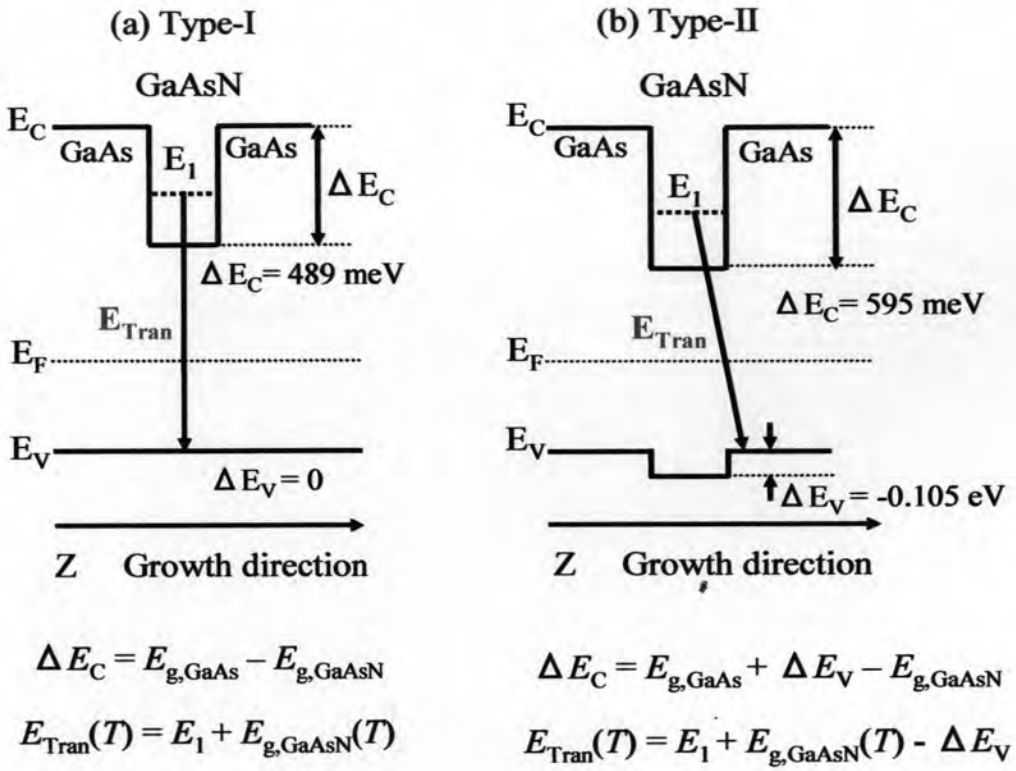

Figure 5.8: Schematic band diagrams of the quantum structures with (a) a type-I and a type-II band alignment and their expected properties.

bandgap energy of GaAsN alloy at 300 K is calculated to be 0.935 eV using the band anticrossing (BAC) model (see detail in section 2.1.2). After that, the bandgap energy of $GaAs_{0.952}N_{0.048}$ alloy at 10 K is calculated using empirical Varshni model. However, in the present case, the value of ΔE_C for $GaAs_{0.952}N_{0.048}$/GaAs QWs structure is approximately determined to be ~ 595 meV, which is much larger than the estimated value of ΔE_C (~ 550 meV) from the difference between the PL peak positions of the annealed $GaAs_{0.949}N_{0.051}$ bulk layer and the GaAs barrier, as shown in Fig. 5.3. In addition, based on HRXRD results, the N concentration inside the $GaAs_{0.949}N_{0.051}$ bulk layer is increased with post-growth thermal annealing treatment (see detail in section 4.2). As a result, we expect that the value of ΔE_C for $GaAs_{0.952}N_{0.048}$/GaAs QWs should be smaller than 550 meV at 10 K because the bandgap energy of GaAsN is decreased with increasing of N concentration. These results strongly suggest that the type-II band lineup may be unable to explain the optical transition in the $GaAs_{1-x}N_x$/GaAs QWs.

Moreover, to confirm this result we calculate the temperature dependence of transition energy, $E_{Trans}(T)$, in GaAsN well layer for QWs type-II band lineup and then compare with those of PL peak position. From Fig. 5.8 (b), the transition energy at any temperature is given by $E_{tran}(T) = E_1 + E_{g,GaAsN}(T) - \Delta E_V$, where $E_{tran}(T)$ is transition energy at any temperature, E_1 is the ground state of the quantization energy in GaAsN well layer, $E_{g,GaAsN}(T)$ is temperature dependence of bandgap energy and ΔE_V is valence band offset of GaAsN/GaAs QWs system. In order to calculate the E_1 in GaAsN well layer, we apply the finite-depth single-square well model to calculate the confinement energies inside the well layer (see section 2.2.2). For simplicity case, we assume that the effective mass of particle in the well (m_w^*) and barrier (m_b^*) are equal to be m^*. From boundary conditions at $z = \pm a$ that φ and $d\varphi/dz$ are continuous, we obtain

$$k_b = k_w \tan k_w a. \tag{5.1}$$

Thus

$$k_w^2 = \frac{2m^*(-|E| + |V|)}{\hbar^2}, \tag{5.2}$$

and

$$k_b^2 = \frac{2m^*|E|}{\hbar^2}, \tag{5.3}$$

where m^* is the effective mass of particle in the well, V is the conduction band offset of GaAsN/GaAs system, a is a half of well width L_z and $\hbar = \frac{h}{2\pi}$, h is Plank's constant. Equation (5.1) can be solved numerically or graphically and the solution gives information about the lowest quantized energy state E_1.

For the tensile strained GaAsN/GaAs QWs, the light-hole state exhibits higher place than the heavy-hole state, inside the well layer. As a consequence, the effective mass of particle inside the well can be determined by reduced masses between the electron effective mass (m^*_e) and light-hole effective mass (m^*_{lh}), which are evaluated at the Brillouin zone center. The m^*_e of $GaAs_{0.952}N_{0.048}$ well layer is calculated to be $0.1128m_0$ using BAC model (see section 2.2.3). On the other hand, the value of m^*_{lh} for $GaAs_{1-x}N_x$ can be approximately determined using a linear interpolation between

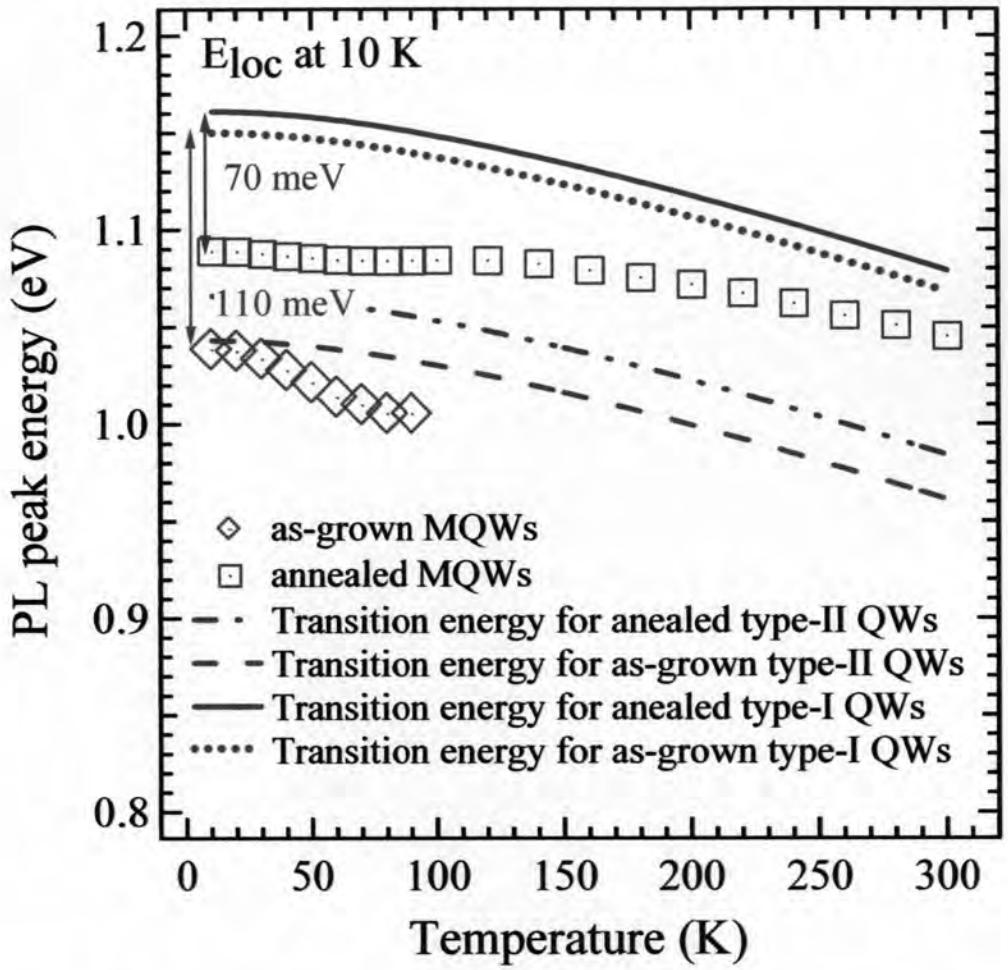

Figure 5.9: Temperature dependence of PL peak position of as-grown and annealed MQWs. The dashed and dashed dotted lines denote the calculated transition energy of as-grown and annealed type-II QWs, respectively. The dotted and solid lines refer to the calculated transition energy of as-grown and annealed type-I QWs, respectively.

the values of m^*_{lh} of GaAs and *c*-GaN. The lists of m^*_e and m^*_{lh} for GaAs and *c*-GaN are summarized in Table 2.1. For $GaAs_{0.952}N_{0.048}$ alloy, the value of m^*_{lh} is determined to be $0.087m_0$. In the case of the $GaAs_{0.952}N_{0.048}$/GaAs type-II band lineup, the ΔE_V and ΔE_C are estimated to be -0.105 eV (see section 2.2.4) and 595 meV, respectively. The temperature dependence of transition energy for the annealed $GaAs_{0.952}N_{0.048}$/GaAs QWs type-II band lineup with well width of 5 nm is calculated to be the dashed dotted line in Fig. 5.9. In comparison with the temperature dependence of PL peak position obtained from the annealed MQW, the calculated transition energy is lower than the PL peak energy over the entire temperature range.

This result indicates that GaAsN/GaAs type-II band lineup may be not capable to explain the optical transition energy in the annealed MQWs. In case of as-grown layer, the calculated transition energy dashed line is shown in Fig. 5.9. The calculated transition energy is relatively comparable with the PL peak position, showing the extremely small localization energy in as-grown MQWs. However, the lowest estimation of the localization energy for annealed MQWs is approximated to be 41 meV, as shown in Fig. 5.7. It is believed that the annealing process can improve the alloy composition fluctuation, indicating that the localization energy for annealed MQWs should be smaller than the as-grown MQWs. These confirmations strongly suggest that the type-II band lineup may be unable to explain the optical transition in the $GaAs_{1-x}N_x$/GaAs QWs.

In addition, it is known that the addition of N into GaAs decreases the bandgap energy, which mainly affects the conduction band (CB) states leading to a large ΔE_C and only a small valence band (VB) discontinuity [44]. Thus, the value of ΔE_V can be approximated to be zero, in our case, so we discuss on the $GaAs_{1-x}N_x$/GaAs type-I band lineup as shown in Fig. 5.8 (a). Accordingly, the value of ΔE_C for the $GaAs_{0.952}N_{0.048}$/GaAs QWs structure, which determined from the difference between E_g (10 K) of GaAs and $GaAs_{0.952}N_{0.048}$/GaAs, as shown in Fig. 5.8 (a), is estimated to be 489 meV. The transition energy is approximated to be the critical transition from the valence band edge to the ground state in the confined energies (see Fig. 5.8 (a)). Then, the calculated transition energy at any temperature for the annealed $GaAs_{0.952}N_{0.048}$/GaAs MQWs type-I band lineup with well width of 5.0 nm is shown as a solid line in Fig. 5.9. It can be seen that the temperature dependence of calculated transition energy is higher than the temperature dependence of PL peak position. This indicates that the GaAsN/GaAs type-I band lineup may be able to explain the optical transition in GaAsN/GaAs QWs. The difference between calculated transition energy and the PL peak position of annealed MQWs is estimated to be localization energy, indicating that the localization energy is estimated to be 70 meV at 10 K. In addition, the energy position of calculated transition energy of as-grown MQWs type-I band lineup is higher than that of the PL peak position over the entire temperature range. The estimated localization energy is approximated to be 110 meV. This value is larger than the localization energy for annealed MQWs, supporting the reduction of localization energy after annealing. These results imply that the calculated transition energy for the type-I band lineup is well consistent with

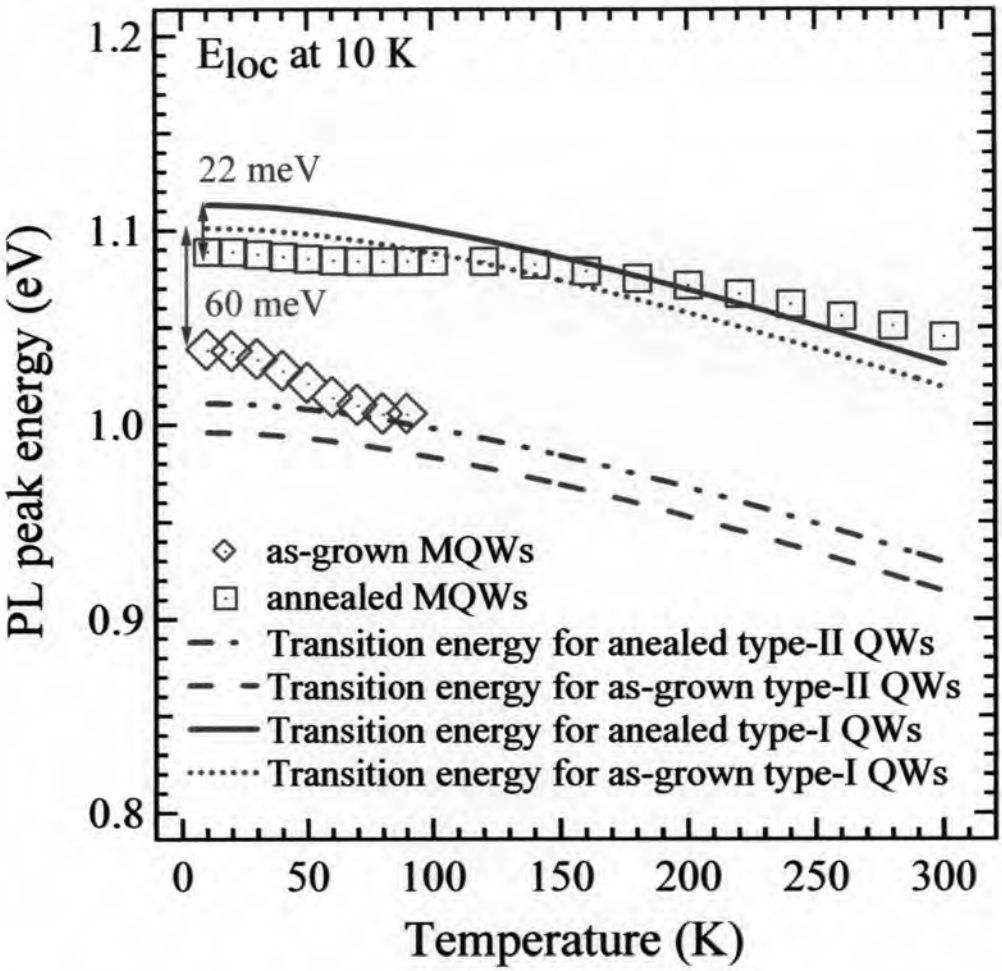

Figure 5.10: Temperature dependence of PL peak position of as-grown and annealed MQWs. In case of the effective mass in the well and barrier is difference, the dashed and dashed dotted lines denote the calculated transition energy of as-grown and annealed MQWs type-II band lineup, respectively. The dotted and solid lines refer to the calculated transition energy of as-grown and annealed MQWs type-I band lineup, respectively.

the experimental results. Finally, we can strongly suggest that the type-I band lineup is a suitable band alignment, describing the optical transition in the $GaAs_{1-x}N_x/GaAs$ QWs structure.

However, it is interesting to know why localization energy in this case is very large. This result may be caused by the estimation of equal effective mass of particle in well and barrier layers. In a real heterostructure, the effective mass of particle in well and barrier layers are different. If this condition is taken into account, the

boundary condition will be continuity of φ and $(1/m^*)d\varphi/dz$ at $z = \pm a$ [35, 36]. So we obtained

$$k_b m_w = k_w m_b^* \tan k_w a, \tag{5.4}$$

and

$$\tan(k_w a) = \frac{m_w^* k_b}{m_b^* k_w}. \tag{5.5}$$

We set

$$x = k_w a, \quad \xi = \frac{m_w^* (2a)^2 V}{2\hbar^2}. \tag{5.6}$$

Thus

$$\tan x = \sqrt{\frac{m_w^*}{m_b^*}} \frac{\sqrt{\xi - x^2}}{x}. \tag{5.7}$$

We can solve solution of Eq. (5.4) by setting $\tan x = y$, and $y = \sqrt{\frac{m_w^*}{m_b^*}} \frac{\sqrt{\xi - x^2}}{x}$ to determine the lowest quantization energy inside the well layer. Figure 5.10 shows the calculated transition energy of as-grown and annealed MQWs. It is evident that the calculated transition energy of as-grown (dashed line) and annealed MQWs (dashed dotted line) type-II band lineup are lower than the PL peak position over the entire temperature range. This also strongly indicates that the type-II band lineup cannot be explained optical transition in GaAsN/GaAs QWs. The calculated transition energy for as-grown and annealed MQWs type-I band lineup are shown in Fig. 5.10 as dotted and solid lines, respectively. It can be seen that the calculated transition energy is higher than the PL peak position over the entire temperature range. This result also strongly suggests that the type-I band lineup can explain optical property in GaAsN/GaAs QWs. Moreover, the localization energy at 10 K of as-grown and annealed MQWs is decreased in this case, suggesting that the calculated transition energy can explain the experimental result.

5.6 Summary

Optical and structural properties of the high N-content $GaAs_{0.950}N_{0.050}$/GaAs MQWs were investigated. The N concentration and well dimension were examined by HRXRD and TEM measurements. The high structural quality of as-grown and annealed $GaAs_{0.950}N_{0.050}$/GaAs MQWs was clearly observed. The PL spectra of the as-grown and annealed $GaAs_{0.950}N_{0.050}$/GaAs MQWs showed a strong emission at 1.04 and 1.09 eV, respectively, around the 1.3 μm-wavelength region. The large conduction band offset ($\Delta E_C \sim 550$ meV) which indicates a large barrier height for an electron confinement in the $GaAs_{0.950}N_{0.050}$/GaAs MQWs was established. After post-growth thermal annealing, the PL peak energy showed a significant blue-shift. Based on HRXRD and TEM results, in such high N-containing MQWs, the PL blue-shift is attributed to the N out diffusion and the improvement of alloy uniformity. These results demonstrate that the possibility of fabricating GaAsN-based optoelectronic devices for optical-fiber communications in the wavelength region around 1.3 μm can be obtained, giving higher efficient PL emission at higher temperatures. The calculated transition energy using the finite-depth single-square well model suggests that the band alignment of the $GaAs_{1-x}N_x$/GaAs QW structure is a type-I band lineup. In addition, the calculated transition energy is close to the experimental result with attention to the difference of effective mass of particle in the well and barrier layers. Moreover, the optical transition energy is originated by the localization potential states, resulting of alloy distribution fluctuation giving rise to the conduction band edge fluctuation and well width fluctuation.